

Supplementary Information

Electrosynthesis of Conducting Mixed-Valence 9,9'-Dimethyl-3,3'-bicarbazyl Rectangular Nanotubes

Katsuyoshi Hoshino,^{*a} Kazuki Takizawa,^a Minako Kubo,^b Katsuyuki Murashiro,^b Nobuyuki Aoki,^a Yuichi Ochiai^a and Hyuma Masu^c

^a Graduate School of Advanced Integrated Science, Chiba University, 1-33 Yayoi-cho, Inage-ku, Chiba 263-8522, Japan

^b Goi Research Center, Chisso Petrochemical Corp., 5-1 Goikaigan, Ichihara, Chiba 290-8551, Japan

^c Chemical Analysis Center, Chiba University, 1-33 Yayoi, Inage-ku, Chiba 263-8522, Japan

Table of Contents

1. Materials and methods	S2
2. Linear sweep voltammetry of 9-methylcarbazole	S2
3. FT-IR spectroscopy of 1-2	S3
4. LDI-TOFMS measurements of 1-2 .	S4
5. XPS measurements of 1-2	S4
6. ¹ H NMR measurement of 1-2	S5
7. ESR measurement of 1-2	S5
8. UV-vis spectroscopy of 1-2	S6
9. Effect of supporting electrolyte type	S7
10. Electrical measurement of 1-2	S8
11. Mechanistic study on the formation of 1-2	S8
12. References	S10

Materials and Methods. 9H-Carbazole (96.0%<), 9-methylcarbazol (99.0%<), 9-ethylcarbazole (97.0%<), and 1-methylpyrrole (99.0%<) were obtained from Tokyo Kasei Kogyo Co. 1-Methylindole (98.0%<) was obtained from Wako Pure Chemicals Co. 9-Octylcarbazole was synthesized according to the literature S1. The tetrabutylammonium salts of ClO_4^- (98%<), BF_4^- (96%<) and PF_6^- (98%<), and lithium perchlorate (99%<) were obtained from Tokyo Kasei Kogyo Co. Methanol (99.8%<), ethanol (99.5%<), acetonitrile (99.7%<), and dichloromethane (99.5%<) of spectroscopic grade were obtained from Kanto Chemicals Co. γ -Butyrolactone (99%<) was obtained from Sigma-Aldrich Co. Water was distilled-deionized water purified by distillation (IWAKI STILL-N1P) and ion exchange (ORGANO G-10 type cartridge).

SEM (Topcon Co., model ABT-32), FE-SEM (Hitachi, model SU-70) and TEM (Hitachi, model H-7650) were used for the structural observations of the samples. Linear sweep voltammetry and controlled-potential electrolysis were carried out using an electrochemical analyzer (ALS, model 600DH). The electric conductivity measurement of the sample film was carried out using the conventional four probe method (Mitsubishi Chemical Analytech Co., Loresta GP MCP-T600 and MCP-TP06P probe).

Laser desorption/ionization (LDI) time-of-flight mass spectroscopy (TOFMS) experiments were performed using a TOFMS spectrometer (Bruker Daltonics Co., autoflex III) operating in the linear and reflector modes. The FT-IR transmission spectra of the samples (KBr pellets) were recorded using a Nicolet 6700 FT-IR spectrometer. For the X-ray photoelectron spectroscopic (XPS) measurements, a ULVAC-PHI model PHI Quantera SXM spectrometer with $\text{Al K}\alpha$ radiation was used. The absolute binding energy scale in the XPS was determined by setting the C 1s signal to 284.6 eV.

The ITO-coated glass plate (Geomatech Co., $10 \Omega/\text{sq}$), Pt plate and saturated calomel electrode (TOA, model HC-205C) were used as the working, counter and reference electrodes, respectively. The ITO-coated glass plates were cleaned by sonication in trichloroethylene, acetone and ethanol (each 10 min.).

Linear sweep voltammetry of 9-methylcarbazole. The linear sweep voltammetry (Fig. S1) of 9-methyl carba-

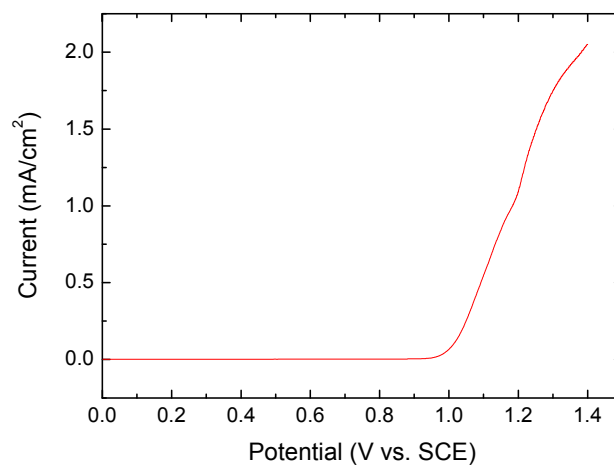


Fig. S1 Linear sweep voltammogram of 10 mM 9-methylcarbazole in a methanol solution containing 0.1 M $\text{TBA}^+\text{ClO}_4^-$ at 20 °C. Sweep rate: 20 mV/s.

zole was carried out using the same solution and electrolytic system as described in the text of this paper. The oxidation current of 9-methylcarbazole began to flow from 1.0 V vs. SCE. Taking into account this result, the potentiostatic oxidation potential was set to 1.1 V as described in the text. As the oxidation potential increased to the anodic side, the number of nanotubes decreased and the flat membrane was formed in priority to the nanotube.

FT-IR spectroscopy of **1-2.** The sample film was prepared on the ITO electrode by the potentiostatic oxidation of 9-methylcarbazol at a potential of 1.1 V ($Q = 40 \text{ mC/cm}^2$) and 20 °C using the solution indicated in Fig. S1. Fig. S2 shows the FT-IR transmission spectra of the **1-2** nanotube sample (a) and the partially-oxidized 9,9'-dimethyl-3,3'-bicarbazyl (b) obtained by the chemical oxidation of 9-methylcarbazol (KBr method). The chemical oxidation was carried out according to the method in the literature S2 and in its supporting information. The ferric chloride was used as an oxidant. Spectra a and b are the same in both the shape and the peak position. The signals at 798 cm⁻¹ and 836 cm⁻¹ observed in spectrum b of the authentic sample correspond to the CH bending of the 1,2,4-trisubstituted aromatic rings of poly(N-alkylcarbazole), which indicates that the carbazole units are bonded by 3-3' coupling.^{S3} The corresponding signals at 797 cm⁻¹ and 834 cm⁻¹ were also observed in spectrum b. The signals^{S3,S4} caused by ClO₄⁻ were observed in both spectra near 1100 cm⁻¹ and 620 cm⁻¹. This is the indication that the building block of **1-2** nanotube contains 9,9'-dimethyl-3,3'-bicarbazyl doped with ClO₄⁻. The signals at 1552 cm⁻¹ in spectrum a and 1558 cm⁻¹ in spectrum b are the ring vibration band characteristics of the oxidized 9,9'-dimethyl-3,3'-bicarbazyl.^{S5} The signals observed near 750 cm⁻¹ and 720 cm⁻¹ are attributed to the CH bending of the 1,2-disubstituted

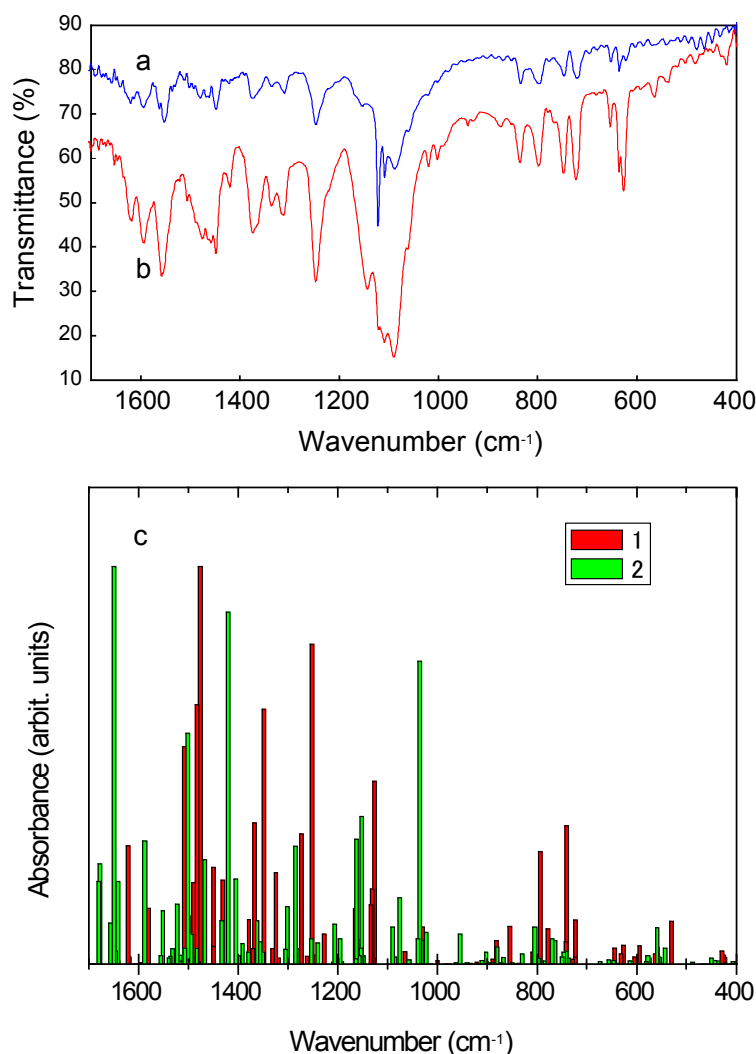


Fig. S2 FT-IR spectra of **1-2** nanotube (a) and partially oxidized 9,9'-dimethyl[3,3']bicarbazyl (b). Panel c shows the spectrum of the 1:1 mixture of **1** and **2** computed using the HF/6-31G* method.

rings.^{S3} Spectrum c in Fig. S2 shows the IR absorption spectrum of the mixture of **1** and **2** calculated by the HF/6-31G* method. The molar mixing ratio of **1** and **2** is 1:1. The black and outlined bars indicate signals caused by **1** and **2**, respectively. In the calculated spectrum, the signal caused by the perchloric acid shifted to the low wavenumber side compared to the experimental spectrum. However, both of the calculated signals caused by **1** and **2** were also observed in the experimental spectrum (spectrum a), which supported that the nanotube consisted of **1** and **2**.

LDI-TOFMS measurements of **1-2**.

The solution indicated in Fig. S1 was used for preparing the

sample film on the ITO electrode by conducting the potentiostatic oxidation of 9-methylcarbazol at a potential of 1.1 V ($Q = 30 \text{ mC/cm}^2$) and 20 °C. The obtained sample was soaked in extrapure water, and dispersed into water by sonication for 1 minute. The test sample was obtained by dropping the dispersed solution on the LDI sample plate, then drying. Fig. S3 shows the LDI-TOFMS spectra (a, linear mode; b, reflector mode) of the **1-2** nanotube sample formed at 20 °C. The spectra indicated signals at $m/z = 359.904$ and 360.086 in the linear and reflector modes, respectively. These values coincided with the molecular weight (360.458) of 9,9'-dimethyl-3,3'-bicarbazyl.

XPS measurements of **1-2**.

The solution indicated in Fig. S1 was used for preparing the sample film on the ITO electrode by conducting the potentiostatic oxidation of 9-methylcarbazol at a potential of 1.1 V ($Q = 100 \text{ mC/cm}^2$) and 20 °C. Fig. S4 shows the XPS spectrum of the N 1s region of the **1-2** nanotube sample. Signals corresponding to N

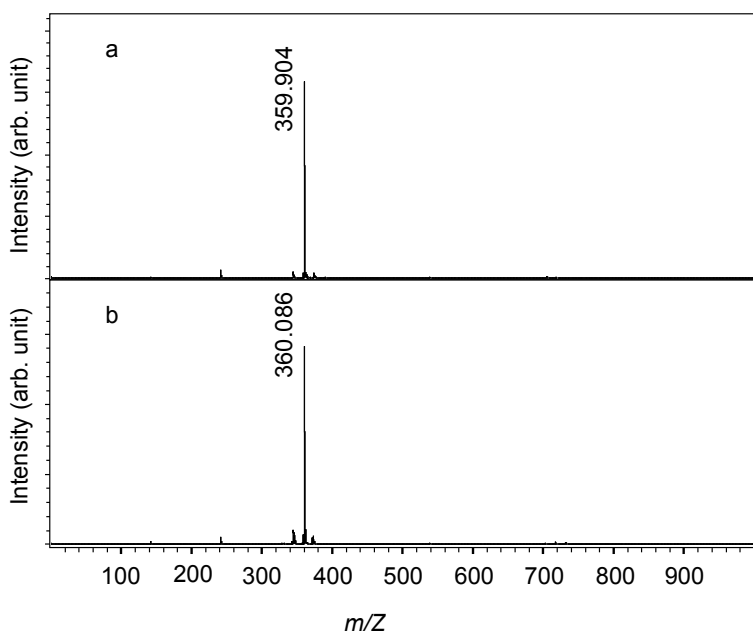


Fig. S3 LDI-TOFMS spectra of **1-2** nanotube in the linear (a) and reflector modes (b).

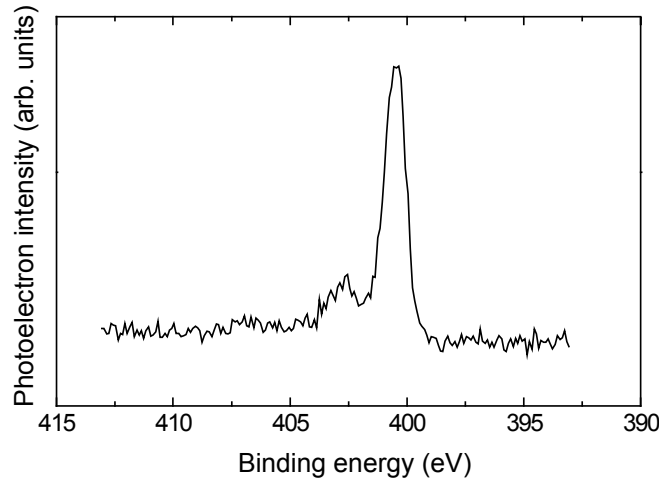


Fig. S4 N1s XPS spectrum for the **1-2** nanotube sample on the ITO.

of the amine nitrogen atom and the quaternary nitrogen atom were observed at 400.35 and 402.66 eV^{S6} respectively. When the waveform separation was carried out and the signal ratio was calculated, the calculated nitrogen atom concentration ratio in the amine and ammonium was 3:1. This means that the ratio of the number of molecules of **1** and **2** in the **1-2** nanotube is 1:1, and suggests that **1** and **2** are alternately stacked to form a mixed valence state.

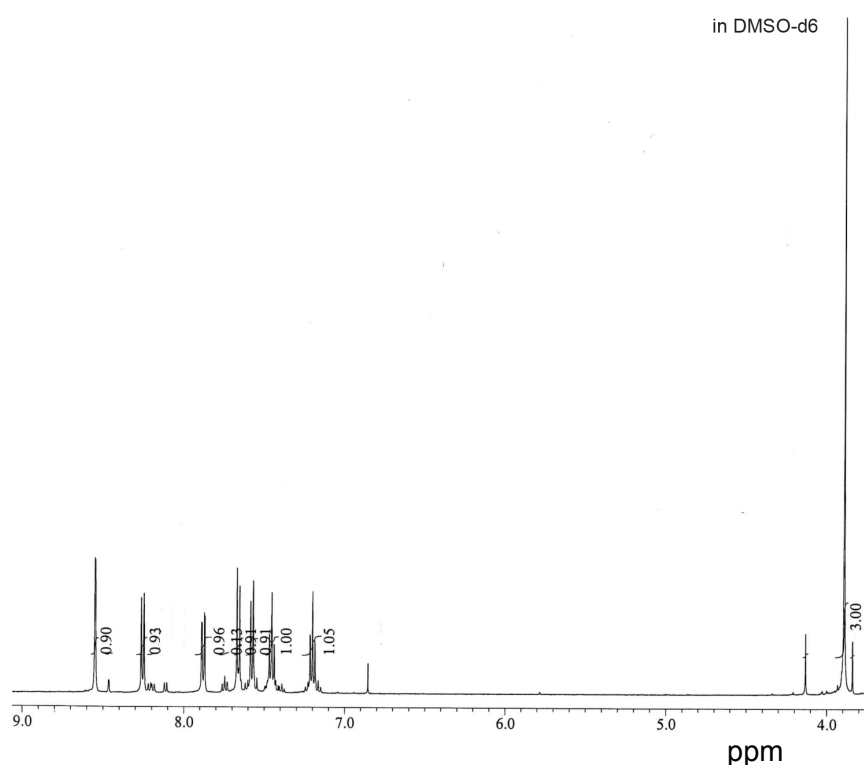


Fig. S5 Selected region of ¹H NMR spectrum of **1-2** in DMSO-d₆.

¹H NMR measurement of **1-2.** The **1-2** nanotube sample was prepared by repetition of the controlled-potential electro-oxidation of 10 mM 9-methylcarbazole in a methanol solution containing tetrabutyl-ammonium perchlorate (0.1 M) at 1.1 V vs SCE. ¹H NMR spectra were recorded in DMSO-d₆ solution with a JEOL JNM-ECA500 spectrometer. All the chemical shifts (δ in ppm) were referenced to the solvent signal. Fig. S5 shows the ¹H NMR spectrum of the **1-2** sample. The spectrum exhibits a peak at 3.89 ppm arising from N-methyl proton (singlet) and seven peaks (7.15–8.55 ppm) in the region of aromatic protons. Based on the comparison of area of proton peaks, six N-methyl protons and fourteen aromatic protons are involved in **1-2**. These peaks, when considered with their splitting, can be assigned to the protons of 9,9'-dimethyl-3,3'-bicarbazyl (**1**).

ESR measurement of **1-2.** The ESR measurement was carried out using the **1-2** powder sample (Fig. S6). ESR spectrum was recorded on a JEOL JES-FA series spectrometer. The g factor value was determined using MnO as an external standard ($g = 2.0058$). Despite the use of a tiny amount of the **1-**

2 sample, an extremely large signal with a g-value of 2.00279 was observed. This g value falls under the category of organic radicals. Additionally, a large peak-to-peak line width suggests that the radical species are delocalized in the large π -conjugation system and coupled with many nuclei. These results clearly demonstrate the presence of radical species, i.e., 9,9'-dimethyl-3,3'-bicarbazylum (**2**).

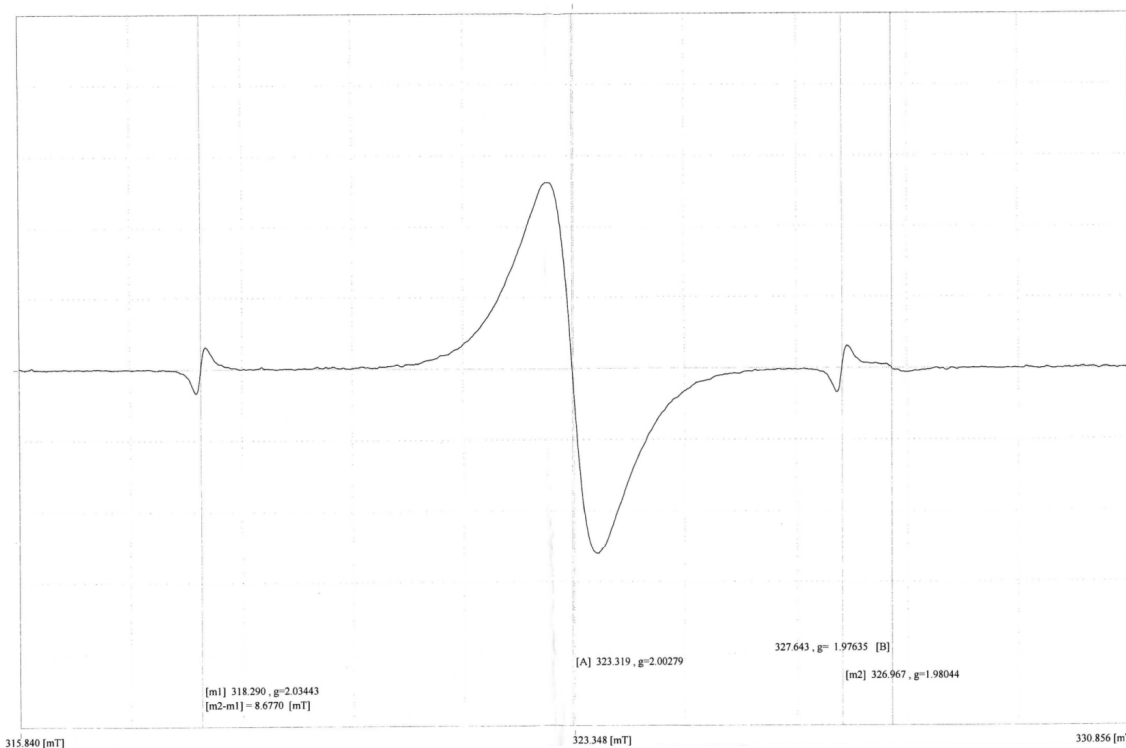


Fig. S6 ESR spectrum of **1-2**.

UV-vis spectroscopy of 1-2. Fig. S7 shows the UV-vis spectra of the **1-2** nanotube samples, which were formed on the ITO electrodes at 20 °C (a) and -10 °C (b). The absorption peaks at 750 nm, 413 nm and 317 nm, respectively, correspond to the electron transitions from the bonding state of polaron to the antibonding state, from the bonding state of the polaron to the π conduction band, and from the valence band to the conduction band.^{S7}

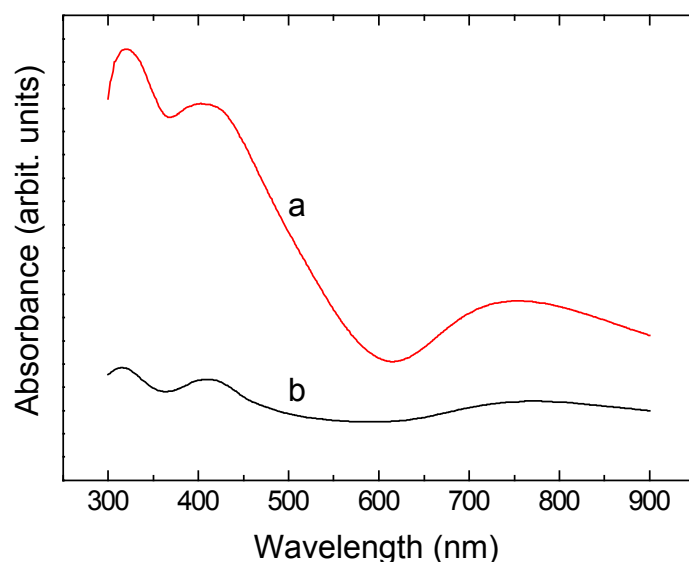


Fig. S7 UV-vis absorption spectra of the **1-2** nanotube samples on the ITO prepared at 20°C (a) and -10°C (b). Q: 30 mC/cm². Electrolysis potential: 1.1 V vs. SCE.

Effect of supporting electrolyte type. The electrolytic oxidation of 9-methylcarbazole was carried out using various supporting electrolytes other than $\text{TBA}^+\text{ClO}_4^-$ as described in the text, and the shapes of their deposits were examined. As supporting electrolytes, the tetrabutylammonium salts of BF_4^- (99% $<$, Tokyo Kasei Kogyo Co.) and PF_6^- (99% $<$, Tokyo Kasei Kogyo Co.), and lithium perchlorate (99% $<$, Tokyo Kasei Kogyo Co.) were used. The conditions of the solution and electrolysis except for the supporting electrolyte were the same as in the case (see text) when $\text{TBA}^+\text{ClO}_4^-$ was used. Fig. S8 shows the SEM images of the

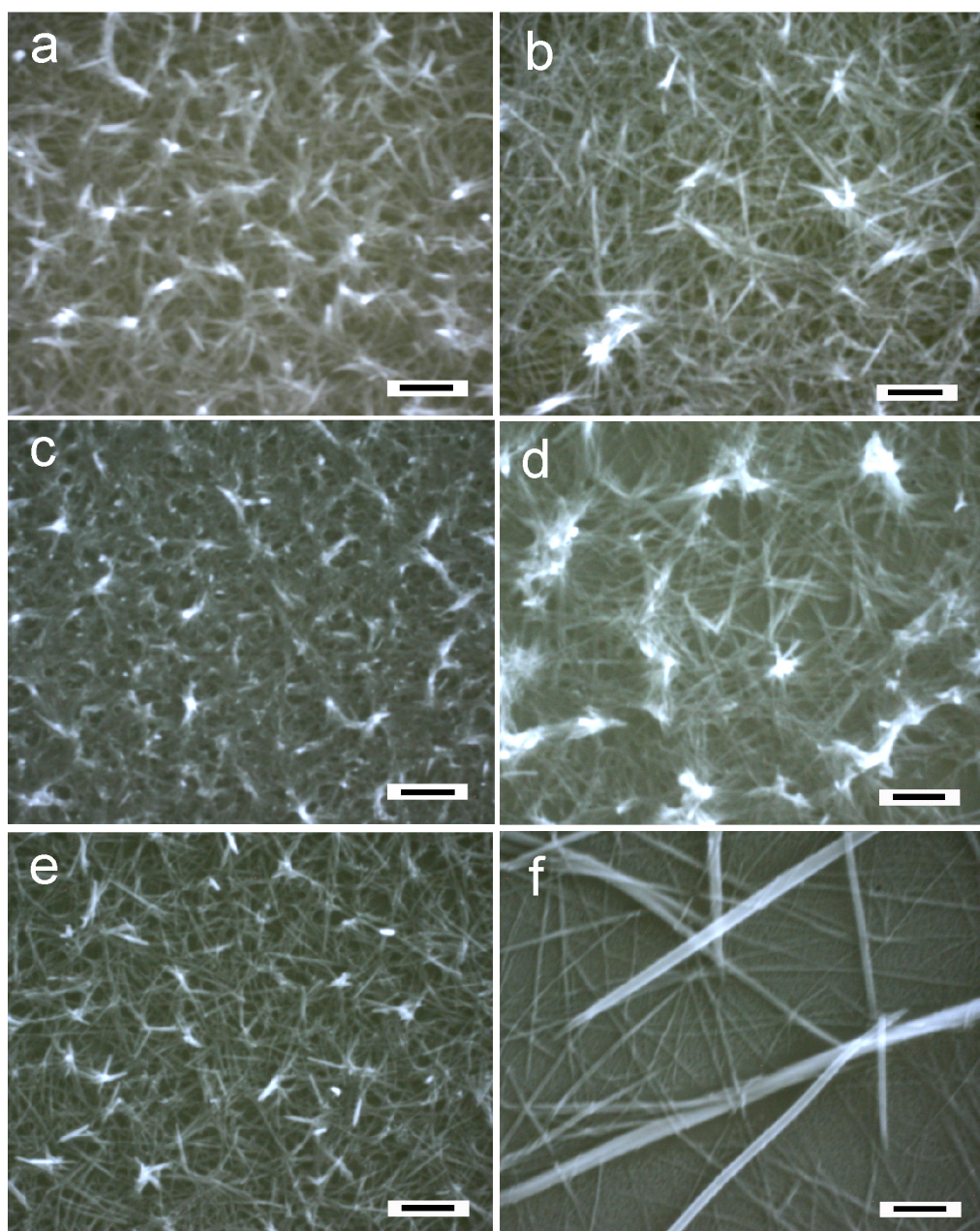


Fig. S8 SEM images of the deposit prepared on the ITO by the electro-oxidation of 10 mM 9-methylcarbazole at 1.1 V vs. SCE in a methanol solution containing 0.1 M of $\text{TBA}^+\text{BF}_4^-$ (a and b), $\text{TBA}^+\text{PF}_6^-$ (c and d) and $\text{Li}^+\text{ClO}_4^-$ (e and f) at 20°C (a, c, and e) and -10°C (b, d, and f). Scale bars: 5 μm .

deposits obtained by the electrolysis using $\text{TBA}^+\text{BF}_4^-$ (a and b), $\text{TBA}^+\text{PF}_6^-$ (c and d) and $\text{Li}^+\text{ClO}_4^-$ (e and f) at 20 °C (a, c, and e) and –10 °C (b, d, and f). When $\text{TBA}^+\text{BF}_4^-$ was used, thin nanotubes similar to the one that was obtained by the electrolysis using $\text{TBA}^+\text{ClO}_4^-$ at 20 °C were obtained by each electrolysis at 20 °C (a) and –10 °C (b). On the other hand, when $\text{TBA}^+\text{PF}_6^-$ was used, thin nanotubes similar to the one that was also obtained by the electrolysis using $\text{TBA}^+\text{ClO}_4^-$ at 20 °C were obtained at both electrolytic temperatures. However, the produced nanotubes interlocked with each other, and a structure like the nanotubes embedded in a flat film was obtained. When the electrolysis was done using $\text{Li}^+\text{ClO}_4^-$, thin tubes at 20 °C and thick tubes at –10 °C were formed, and this result was same as the case using $\text{TBA}^+\text{BF}_4^-$. This indicates that the anion part of the supporting electrolyte influences the association characteristics of the **1-2** nanotube.

Electrical measurement of 1-2. Part a in Fig. S9 shows the electrical measurement configuration (two-terminal configuration)^{S8} for the bottom-contacted **1-2** nanotube device. The **1-2** nanotubes were prepared by the electro-oxidation of 9-methylcarbazol at a potential of 1.1 V ($Q = 300 \text{ mC/cm}^2$) and 20 °C, and were mechanically transferred onto prepatterned Pd microelectrodes of 50-nm thick and 3-μm gap on oxidized silicon chip substrate. The sample was installed in a probe station and a source-drain current (I_{SD}) was measured by applying a source-drain voltage (V_{SD}) and a back gate voltage (V_{BG}). Part b shows the SEM image of the bottom-contacted device. Part c shows the current-voltage ($I_{SD}-V_{SD}$) characteristic of the device shown in part b measured in a two-terminal configuration. Almost linear $I_{SD}-V_{SD}$ response was obtained, with a corresponding conductivity of approximately $2.3 \times 10^{-5} \text{ S/cm}$. Note that the conductivity value represents a lower bound since it involves the contributions from the contact resistances between the nanotube and the source electrode and between the nanotube and the drain electrode. The electric conductivity value was therefore lower than that of the polycarbazole film ($10^{-4} \sim 10^{-3} \text{ S/cm}$)^{S4,S9} prepared by electropolymerization. However, neither photo-current nor back-gate voltage (V_{BG}) response was observed, suggesting a metallic character.

Mechanistic study on the formation of 1-2. Although the mechanism of the **1-2** nanotube formation could not be clarified, important data for determining the mechanism are as follows. Fig. S10 shows an SEM image of the deposit formed on the ITO substrate by the electrochemical oxidation (applied potential: 1.1 V vs. SCE, $Q = 30 \text{ mC/cm}^2$) of 9-methylcarbazole at –10 °C. Part a shows the nanosheet structure of the deposit. A rolling mechanism that such a nanosheet or nanobelt is the precursor of the nanotube structure and it curls to form a nanotube has been reported.^{S10} On the other hand, a barnacle-shaped or bowl-shaped core existed at the foot of the nanotube, and nanotubes were observed that grew in portions at which multiple cores had accumulated (Part b in Fig. S10). At present, the nanotube formation mechanism, which contains the simultaneous formation of these two structures, cannot be considered. However, we hope to elucidate the mechanism by further examining the nanotube material or promoting the chemical analysis of

nanotubes in the future.

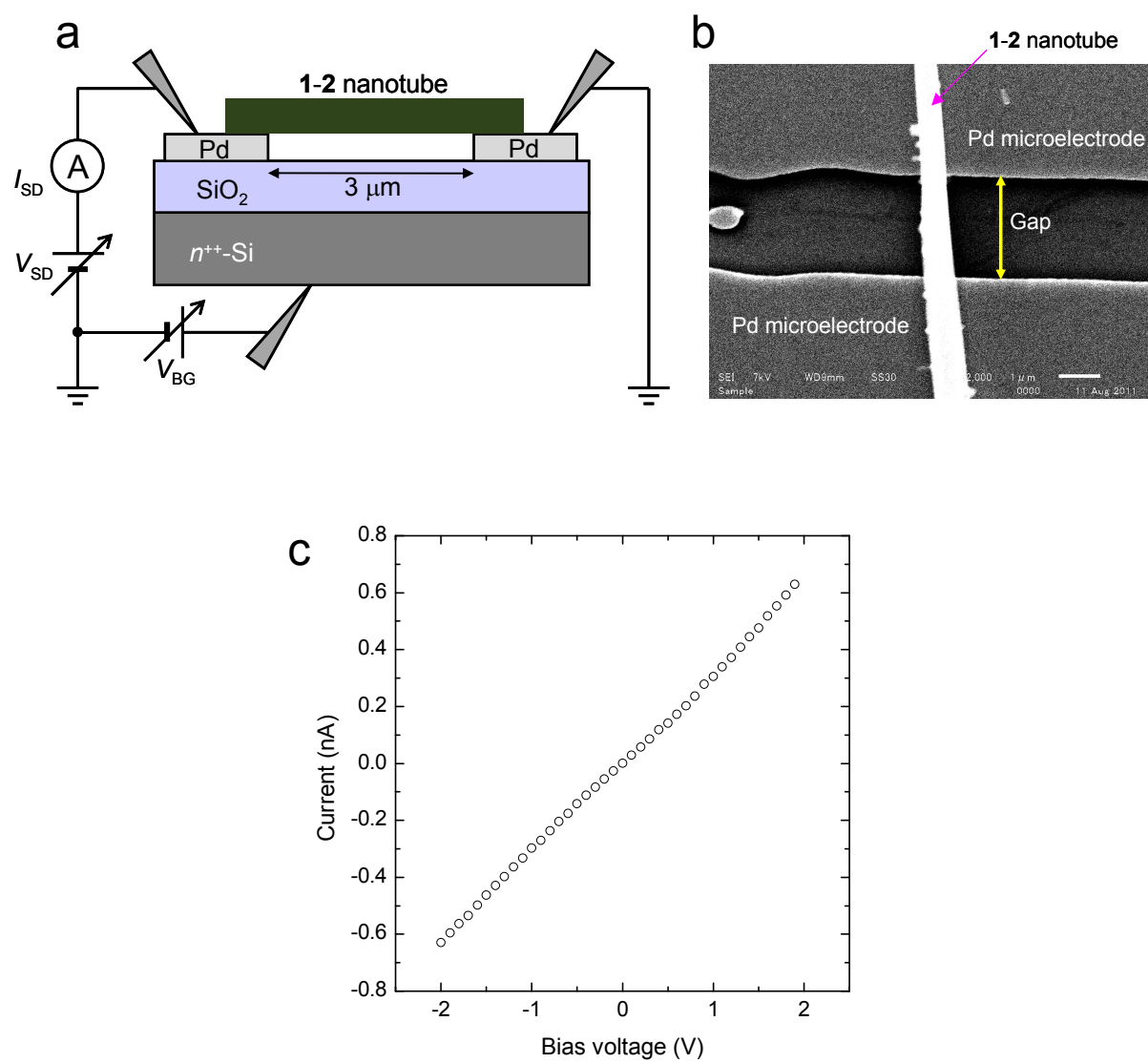


Fig. S9 a) Schematic of a bottom-contact nanotube device. b) SEM image of the device. Scale bar: 1 μm. c) current-voltage ($I_{SD}-V_{SD}$) characteristic of the single **1-2** nanotube in the dark.

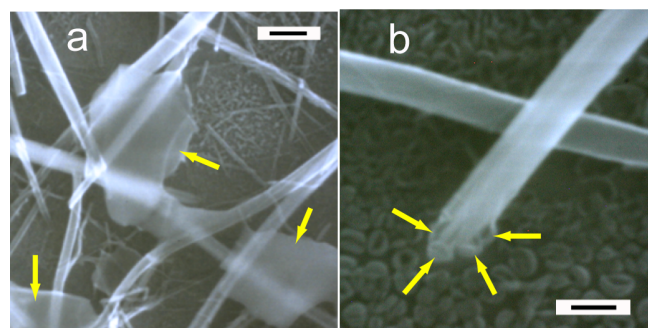


Fig. S10 (a) SEM image of the deposit on the ITO prepared by the electro-oxidation of 10 mM 9-methylcarbazole in methanol at -10 °C and 1.1 V vs. SCE ($Q = 30 \text{ mC/m}^2$). Scale bar: 2 μm . (b) SEM image of the deposit on the ITO prepared by the electro-oxidation of 50 mM 9-methylcarbazole in methanol at -10 °C and 1.1 V vs. SCE ($Q = 30 \text{ mC/m}^2$). Scale bar: 1 μm .

References

- S1 A. Langendoen, J. P. M. Plug, G.-J. Koomen, U. K. Pandit, *Tetrahedron*, 1989, **45**, 1759.
- S2 K. Brunner, A. Dijken, H. Börner, J. J. A. M. Bastiaansen, N. M. M. Kiggen, B. M. W. Langeveld, *J. Am. Chem. Soc.*, 2004, **126**, 6035 and its supporting information.
- S3 S. Cattarin, G. Mengoli, M. M. Musiani, B. Schreck, *J. Electroanal. Chem.*, 1988, **246**, 87.
- S4 E. Sezer, B. Ustamehmetoglu, A. S. Saraç, *Synth. Met.*, 1999, **107**, 7.
- S5 A. Zahoor, T. Qiu, J. Zhang, X. Li, *J. Mater. Sci.*, 2009, **44**, 6054.
- S6 A. D. Monvernay, P. C. Lacaze, J. E. Dubois, *J. Electroanal. Chem.*, 1981, **129**, 229.
- S7 M. M. Verghese, T. Basu, B. D. Malhotra, *Mater. Sci. Engn.*, 1995, **C3**, 215.
- S8 (a) G. A. O'Brien, A. J. Quinn, D. A. Tanner, G. Redmond, *Adv. Mater.*, 2006, **18**, 2379; (b) Q. Tang, L. Jiang, Y. Tong, H. Li, Y. Liu, Z. Wang, W. Hu, Y. Liu, D. Zhu, *Adv. Mater.*, 2008, **20**, 2947.
- S9 (a) S. Cattarin, G. Mengoli, M. M. Musiani, B. Schreck, *J. Electroanal. Chem.*, 1988, **246**, 87; (b) A. S. Saraç, E. Sezer, B. Ustamehmetoglu, *Polym. Adv. Technol.*, 1997, **8**, 556.
- S10 (a) R. Tenne, L. Margulis, M. Genut, G. Hodes, *Nature*, 1992, **360**, 444; (b) Y. D. Li, X. L. Li, R. R. He, J. Zhu, Z. X. Deng, *J. Am. Chem. Soc.*, 2002, **124**, 1411; (c) C. Ye, G. Meng, Z. Jiang, Y. Wang, G. Wang, L. Zhang, *J. Am. Chem. Soc.*, 2002, **124**, 15180; (d) X. Gou, F. Cheng, Y. Shi, L. Zhang, S. Peng, J. Chen, P. Shen, *J. Am. Chem. Soc.*, 2006, **128**, 7222; (e) C. Ye, Y. Bando, G. Shen, D. Golberg, *Angew. Chem. Int. Ed.*, 2006, **45**, 4922; (f) B. Geng, F. Zhan, H. Jiang, Y. Guo, Z. Xing, *Chem. Commun.*, 2008, 5773; (g) Z. D. Zujovic, C. Laslau, G. A. Bowmaker, P. A. Kilmartin, A. L. Webber, S. P. Brown, J. Travas-Sejdic, *Macromolecules*, 2010, **43**, 662.